Construction and Building Materials 233 (2020) 117200

Contents lists available at ScienceDirect

Construction and Building Materials

journal homepage: www.elsevier.com/locate/conbuildmat

Effectiveness of one-to-one phosphate to chloride molar ratio at different chloride and hydroxide concentrations for corrosion inhibition of carbon steel

Danial Iravani, Reza Arefinia *

Chemical Engineering Department, Faculty of Engineering, Ferdowsi University of Mashhad, Mashhad, Iran

HIGHLIGHTS

- At a critical pH named passivation pH (pHp), the corrosion state changes from active to passive.
- An increase in the amounts of chloride and phosphate at $R = 1$ causes a decrease in pH_p.
- At pH > pHp, resistance to pitting corrosion significantly increases.
- The phosphate inhibition depends strongly on the amounts of both phosphate and chloride ions.
- The inhibition mechanism of phosphate is processed by the formation a duplex layer passive film.

ARTICLE INFO

Article history:
Received 13 June 2019
Received in revised form 3 October 2019
Accepted 7 October 2019
Available online xxxx

Keywords:
Carbon steel
Phosphate
Solution pH
Chloride contamination
Passivation

ABSTRACT

In this work, the impact of pH on the corrosion inhibition of carbon steel by phosphate ions in solutions with different contaminations of chloride ions (1, 10, and 100 mmol L^{-1}) with 1:1 phosphate to chloride molar ratio was investigated using electrochemical methods including potentiodynamic polarization and electrochemical impedance spectroscopy (EIS). Moreover, the electrochemical results were complemented using surface analysis methods, including scanning electron microscopy (SEM), energy dispersive spectroscopy (EDS), Raman spectroscopy, and Fourier transform infrared (FTIR) spectroscopy. The obtained results showed that at the passivation pH (pH_p), the corrosion state changes from active to passive. The value of pH_p decreases with an increase in the concentration of phosphate ions and the protection against both uniform and pitting corrosion in the long term was improved. The phosphate inhibition on the carbon steel surface processed through the formation of a duplex layer, including iron (hydro)oxides (inner part) and iron phosphate complexes (outer part).

1. Introduction

Corrosion phenomenon of steel in different environments may cause some serious industrial problems, and using of corrosion inhibitor is a promising method to prevent or minimize the destructive effects [1–3]. Among various types of inhibitor, phosphate compounds as the inorganic inhibitors have some advantages, including low cost and low toxicity [4–7]. Therefore, various phosphate compounds such as trisodium phosphate (Na_3PO_4), disodium hydrogen phosphate (Na_2HPO_4), and disodium monofluoride phosphate (Na_2PO_3F) have been used to control the corrosion process in various applications such as concrete [3–5,8–15], drinking water distribution system [16], cooling water systems [17], and boilers [18,19].

Many studies have been accomplished to understand the inhibition performance of phosphate on the iron surface in different environments [20–23]. Generally, it has been accepted that the passive film, formed on the iron surface in alkaline solution, consists of a duplex layer where the inner part is composed of iron(hydro)oxides and the outer part from iron phosphate complexes such as ferrous hydrogen phosphate ($FeHPO_4$), ferrous phosphate $Fe_3(PO_4)_2$, and ferric phosphate ($FePO_4$) [24–26]. However, the nature of this passive film depends on the various factors namely solution pH, solution temperature, and chloride concentration [1,27,28].

In the case of concrete application, the effect of phosphate on the corrosion inhibition of steel reinforcement has been extensively investigated by Dhouibi et al. [29,30] and Yohai et al. [5,10,25]. In this regard, some researchers suggested that phosphate acts as a

* Corresponding author.
E-mail address: arefinia@um.ac.ir (R. Arefinia).

https://doi.org/10.1016/j.conbuildmat.2019.117200
0950-0618/

cathodic inhibitor if the concentration ratio of phosphate to chloride (R ratio) becomes less than 0.6 [2,4,29,30], while some others believed that at sufficiently high concentration of phosphate (R >0.6) the inhibition mechanism of phosphate is as anodic [6,30] or even mixed [5,10]. In this regard, there is a general agreement in the literature that an increase in the R ratio up to 1 improves the resistance against both general and pitting corrosion [25,30,31]. Therefore, some researchers studied the inhibition behavior of phosphate in a 1:1 phosphate to chloride molar ratio [5,6] which is also an appropriate ratio from the economics standpoint.

These studies on the phosphate, as an inhibiting agent for concretes, have been performed only in highly alkaline solutions (pH about 12), simulating the chemical environment of concrete pores or in mildly alkaline solutions (pH about 9), corresponding to the carbonated solutions. However, these findings are valid mainly in solutions with high chloride contamination. Recently, Ben Mansour et al. [8] assessed the effect of chloride contamination in terms of $[Cl^-]/[OH^-]$ ratio on the efficiency of phosphate against prestressed steel corrosion in a highly alkaline solution, simulated concrete pore solution, who found that the critical $[Cl^-]/[OH^-]$ ratio increases in presence of phosphate ions. In our previous work, the corrosion inhibition of carbon steel by dipotassium hydrogen phosphate (K_2HPO_4) in both mildly and high alkaline solutions, contaminated with low chloride concentration, was investigated where it was reported that only at a critical phosphate concertation, the passive film could be formed on the metal surface [24].

In practical, an increase in the chloride concentration and pH solution within the concrete pores occurs mainly due to the diffusion process of chloride ions and hydroxyl groups. Although, it may take a long time until reach to a high level which was studied by Nahali et al. for the diffusion of chloride ions [9]. Moreover, phosphate ions may be used as a corrosion inhibitor in different applications such as boilers [18,32] and cooling water systems [17,24], where the metal can be subjected to an electrolyte with different chloride concentrations and pH values. Nevertheless, according to the best our knowledge, no detailed study has been done on the effect of chloride concentration and pH, in a wide range of variations, on the phosphate behavior as a corrosion inhibitor.

The aim of this work is devoted to study the effectiveness of phosphate ions as corrosion inhibitor for carbon steel. The effect of solution pH, varying in an alkaline range (from 9 to 12) and chloride ions in a wide range of chloride concentration, on the corrosion inhibition of carbon steel by phosphate ions was investigate. To this end, the one-to-one phosphate to chloride molar ratio was chosen for all solutions. Also, chloride was incorporated into the solutions in different concentrations including 1, 10, and 100 mmol L^{-1}, corresponding to the different applications: with low (e.g., boilers) [32,33], moderate (e.g., cooling water systems) [17,34], and high level (e.g., concrete) [5,25] of chloride contamination. The corrosion behavior of carbon steel was studied using the electrochemical methods of potentiodynamic polarization and electrochemical impedance spectroscopy (EIS) together with different surface analysis techniques including scanning electron microscopy (SEM), energy dispersive spectroscopy (EDS). Moreover, the phosphate inhibition in the long term was evaluated using weight loss measurement and the corrosion products were analyzed by Raman spectroscopy and Fourier transform infrared (FTIR) spectroscopy.

2. Experimental

2.1. Materials and electrolyte

The chemical composition of carbon steel grade SA-106 was used as working metal is presented in Table 1. The cubic shape specimens with a dimension of 1 cm × 1 cm × 1 cm were mounted with epoxy resin, so the remaining surface area was 1.0 cm^2. The surface of specimens was polished with a series of silicon carbide emery paper up to grade 2000 [24,34,35] to minimize the effect of surface roughness which may be necessary in the case of the specimens with the small surface area. After that, they were degreased with acetone and rinsed with double distilled water. Finally, to prevent any corrosion occurrence, the surface of specimens was immediately dried with warm air [30,34,36].

The chemical substances, including disodium hydrogen phosphate (Na_2HPO_4) as a corrosion inhibitor and sodium chloride (NaCl) to provide chloride as the aggressive ion were supplied by Merck Co. with analytical grade. The electrolyte solutions were prepared in double distilled water by addition of equal phosphate and chloride concentration (R = 1) where three chloride phosphate solutions (CPS) were prepared at the concentrations of 1 mmol L^{-1} (CPS1), 10 mmol L^{-1} (CPS10), and 100 mmol L^{-1} (CPS100). The values of solution pH (9, 10, 11, and 12) were adjusted by NaOH and all electrochemical tests were carried out at room temperature (25 ± 2 °C).

2.2. Electrochemical measurements

All electrochemical measurements were performed using Autolab potentiostat/galvanostat (PGSTAT 302N) in a glass vessel containing 100 mL electrolyte and three electrodes: a saturated calomel electrode (SCE) as reference electrode, a platinum electrode as auxiliary electrode, and the mounted carbon steel as working electrode. All electrochemical measurements were carried out at least three times until a good reproducibility was obtained.

The potentiodynamic polarization test was performed according to ASTM G 5–94 [37] at which potential was swept from −400 mV below OCP towards noble direction until reach the pitting or oxygen evolution potential with scan rate of 20 mV/min after 24 h immersion of working electrode in electrolyte [5,10,25]. In the case of the active state of corrosion, the polarization parameters including corrosion current density (i_{corr}) and corrosion potential (E_{corr}) were estimated by the implementation of Tafel extrapolation at the potential range about 100 mV far from the E_{corr} where a linear behavior (Tafel region) is observed for at least one decade. However, for the passive state of corrosion, i_{corr} and E_{corr} have the same meaning of passive current density and passive potential, respectively, determined using the region at which the corrosion current density does not change with potential sweep. Therefore, the value of cathodic Tafel slope (β_c) was estimated for all systems, while the anodic Tafel slope (β_a) was meaningful only for the systems with an active state of corrosion.

The electrochemical impedance spectroscopy (EIS) was conducted according to ASTM G 106-89 [38] after 24 h immersion when a steady condition was achieved. Then the EIS test was performed at OCP with AC perturbation amplitude of ± 10 mV in the frequency range from 100 kHz to 10 mHz.

2.3. Weight loss measurements

The weight loss test was performed for 120 days immersion of the carbon steel coupons at room temperature according to the guidelines in ASTM D 2688 [39]. To do this, two polished rectangular shapes of carbon steel coupons with a dimension of 2 cm × 2 cm × 1 cm were used. The series of silicon carbide emery paper of grades up to 800 were used to polish the coupons, which may be a suitable grade for the high surface of coupons relative to that used for the electrochemical tests. After that, coupons were washed by acetone and double distilled water. Finally, they were precisely weighed by a balance with the precision of 3 digits before immersion. After 120 days immersion, the coupons were taken out

Table 1
Chemical composition of carbon steel A106.

Elements	C	Mn	P	S	Si	Cr	Cu	Mo	Ni	V	Fe
Composition wt. %	0.35	1.06	0.04	0.04	0.10	0.40	0.40	0.15	0.40	0.08	balance

and dried to perform Raman spectroscopy. Then, the corrosion products were removed mechanically, washed by immersion in HCl 1 mmol L^{-1}, neutralized with a saturated Na_2CO_3 solution, rinsed with double distilled water, then dried and reweighted.

2.4. Surface and corrosion product analyses

The scanning electron microscopy (SEM, MIRA3 TESCAN) and energy dispersive spectroscopy (EDS) were used to assess the pitting corrosion state and elemental analysis of metal surface, respectively, after potentiodynamic polarization.

After weight loss measurement, corrosion products formed on the coupons during immersion time were characterized by ex-situ Raman spectroscopy using an AvaRaman-785 TEC with a 785 nm laser wavelength, exposure time 15 s and laser power 500; additionally, Raman spectroscopy was done on some different parts of corrosion products with reproducible results. Furthermore, Fourier transform infrared spectroscopy (FTIR) in the range 400–2000 cm^{-1} was recorded using Thermo-Nicolet Avatar 370 to study the nature of corrosion products.

3. Results and discussion

3.1. Potentiodynamic polarization

The effect of solution pH, varying from 9 to 12, on the corrosion behavior of carbon steel in CPS1, CPS10, and CPS100 corresponding to 1, 10, and 100 mmol L^{-1} of equal concentration of chloride and phosphate ($R = 1$) was investigated using the potentiodynamic polarization experiment and the obtained results are shown in Fig. 1a through c. It is evident that an increase in the concentration of hydroxyl groups creates a tendency to shift the corrosion state from active to passive where the complete passivation of carbon steel was established at pH $\geq$ 11 for CPS1 and pH $\geq$ 10 for CPS10, while in the case of CPS100, the metal surface becomes passivate at pH $\geq$ 9. Note that in CPS100, the polarization test at pH = 8 showed an active-passive state of corrosion (figure not shown). Therefore, there is a critical pH named as passivation pH (pH_p) at which the system is early passivated by increasing the concentration of hydroxyl groups. In other words, at pH $\geq$ pH_p, the corrosion behavior of metal will be as the passive state and when pH $\leq$ pH_p, an active state of corrosion will be observed. Moreover, pH_p is a significant parameter in the view of both general and pitting corrosion, and when pH $\leq$ pH_p, the inhibitor will be unable to protect the metal surface, efficiently.

These results suggest that the amounts of both chloride and phosphate, besides their concentration ratio, have a significant effect on the corrosion behavior of carbon steel i.e. for an equal increase in the concentration from 1 to 100 mmol L^{-1} favors the passivation of the carbon steel at the lower pH values.

The polarization parameters for the curves shown in Fig. 1, are presented in Table 2. For the active state of corrosion, the polarization parameters were determined using Tafel analysis, while in the case of a passive state the McCafferty method was applied correctly [40].

From Table 2, at pH_p for CPS1, CPS10 and CPS100, the ratio of $[Cl^-]/[OH^-]$ is equal to 1, 10^2, and 10^4, respectively. When the concentration of both chloride and phosphate ions increases one order of magnitude, the passivation of the metal surface is established in one order of magnitude lower concentration of hydroxyl groups. Therefore, these results point the fact that when the concentration of phosphate and chloride simultaneously increases, the passivation effect of phosphate ions on the metal surface is superior to the deterioration effect of chloride ions on the passive film.

Inspection in Table 2 reveals that at a constant pH, one can find also a critical phosphate concentration at which the passive state is made on the metal surface as discussed in previous work [24]. In detailed, Table 2 shows that at $R = 1$ when pH decreases from 11 to 9, a higher amount of phosphate is required to keep the passive state on the metal surface and hence, the critical phosphate concentration shifts from 1 to 100 mmol L^{-1}.

Moreover, it can be found from Table 2 that for all solutions, an increase in pH up to pH_p is associated with a decrease in i_{corr} value and a shift of E_{corr} to more noble values; however, a reverse trend of variations is observed by further increase in solution pH (pH > pH_p). Therefore, the lowest value of i_{corr} and the most positive value of E_{corr} are attained at pH_p. At the same time, the cathodic Tafel slope (β_c) slightly reduces, suggesting the facilitation of cathodic reaction. An increment in the value of anodic Tafel slope (β_a) with pH in the active state can be considered as an indication of the enhancement in the tendency to passivate the metal surface. The relatively high value of i_{corr} in some passive conditions can be related to the structure of passive film which needs to be further studied.

In the case of pitting corrosion, at pH > pH_p, the increase of solution pH provides a significant increase in the value of pitting potential (E_{pit}), suggesting the higher resistance of passive film against the chloride attack. Although, it should be noted that for the E_{pit} value higher than oxygen evolution potential (at pH = 12 when E_{pit} > 277 mV_{SCE}) the increase of anodic current is related to the oxygen evolution phenomenon [41].

To describe the passivation and pitting mechanism, it must be noted that generally there is a balance between two processes: phosphate species and hydroxyl groups are adsorbed on the metal surface and thereby estabilize the passive film against breakdown while the aggressive ions of chloride penetrate within the structure of passive film and induce its deterioration [11,40]. Moreover, it was reported that the small radius of sodium ions and their lower binding capacity of chloride compared to other cations e.g., Mg^{2+} facilitates the diffusion of chloride ions and hence accelerates the pitting phenomenon [42]. Therefore, prior to the pitting potential, the effect of phosphate ions is dominant, while after the pitting potential, chloride ions breaks down the passive film at local points. In this situation, the corrosion current density suddenly increases as a result of acceleration in the metal dissolution.

In the case of phosphate inhibitor, variation of solution pH affects also on the concentration of different forms of phosphate anions. For the pH range, selected in the present work and on the basis of different acid dissociation constants (K_a), it can be stated that at pH = 9, hydrogen phosphate anion (HPO_4^{2-}) is the most important form with a mole fraction of about 0.93 from total phosphate species. However, the increase of pH leads to the gradually conversion of HPO_4^{2-} to phosphate anions (PO_4^{3-}) and at pH = 12, the phosphate species is mainly in the form of PO_4^{3-} with a mole fraction of about 0.98 [24]. According to these concepts, it can be deduced that the variation of solution pH causes a competitive adsorption between different forms of phosphate which creates a change in the nature of passive film where the iron/phosphate complexes of $FeHPO_4$ and $Fe_3(PO_4)_2$ are mainly formed in mildly

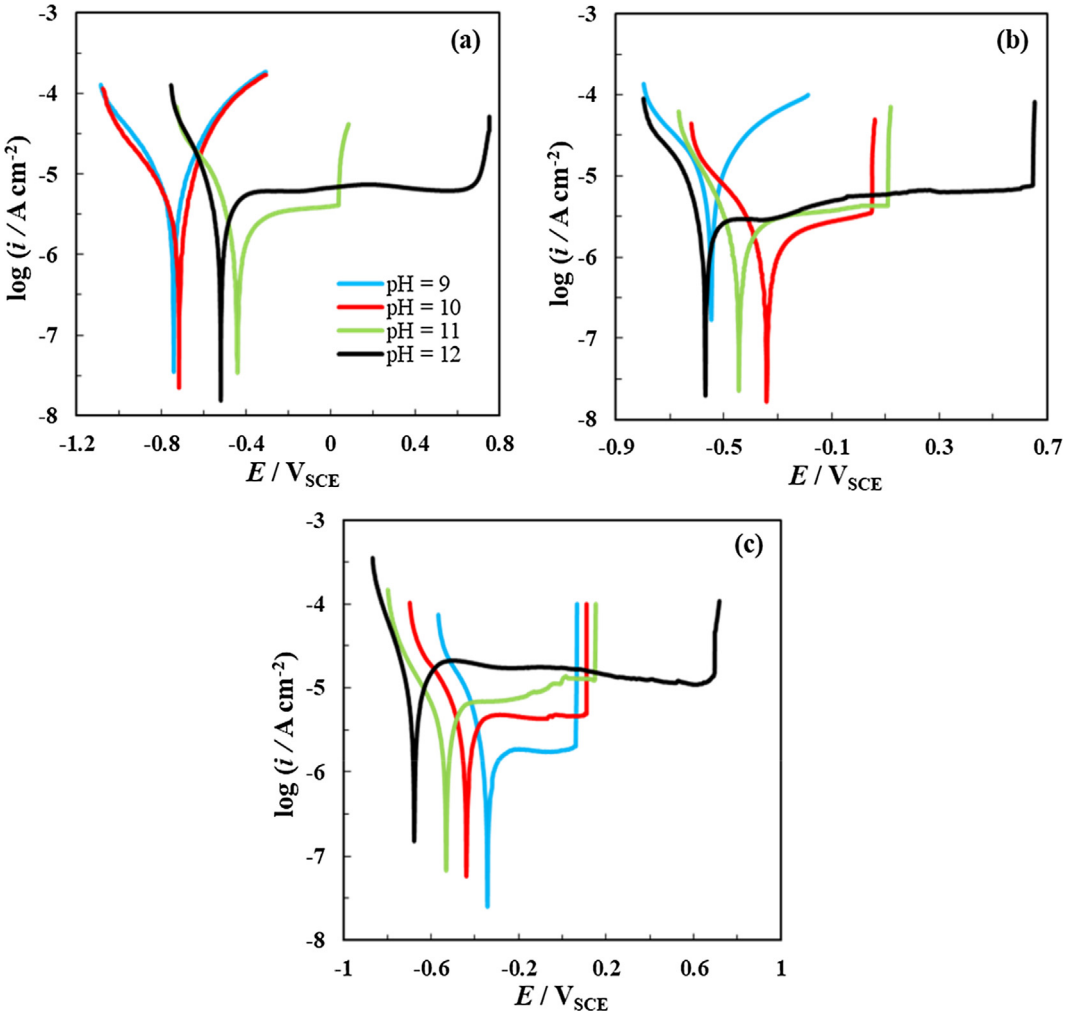

Fig. 1. Effect of pH on the potentiodynamic polarization curves for carbon steel in various solutions: (a) CPS1, (b) CPS10, and (c) CPS100 at room temperature. Scan rate: 20 mV min^{-1}.

Table 2
The average value of polarization parameters for corrosion of carbon steel in CPS1, CPS10, and CPS100 at different pH values and at 25 °C.

Solution	pH	Corrosion State	E_{corr} (mV_{SCE})	i_{corr} (μA cm^{-2})	β_c (mV/dec)	β_a (mV/dec)	E_{pit} (mV_{SCE})
CPS1	9	Active	−741 ± 14	6.2 ± 0.3	−298 ± 10	180 ± 8	–
	10	Active	−712 ± 11	4.2 ± 0.1	−260 ± 7	199 ± 5	–
	11	Passive	−439 ± 15	2.3 ± 0.2	−163 ± 8	–	40 ± 14
	12	Passive	−519 ± 16	5.4 ± 0.3	−188 ± 20	–	674 ± 9
CPS10	9	Active	−545 ± 9	5.6 ± 0.3	−277 ± 19	266 ± 18	–
	10	Passive	−340 ± 8	2.1 ± 0.2	−194 ± 4	–	50 ± 7
	11	Passive	−467 ± 7	2.6 ± 0.2	−202 ± 11	–	110 ± 15
	12	Passive	−568 ± 6	6.2 ± 0.3	−233 ± 13	–	650 ± 12
CPS100	9	Passive	−348 ± 18	1.8 ± 0.2	−108 ± 16	–	57 ± 9
	10	Passive	−430 ± 16	4.6 ± 0.3	−220 ± 18	–	108 ± 13
	11	Passive	−531 ± 9	5.9 ± 0.2	−222 ± 12	–	147 ± 7
	12	Passive	−676 ± 7	20.3 ± 0.2	−121 ± 6	–	688 ± 6

and highly alkaline solution, respectively [6,24]. This will be further studied later.

3.2. Electrochemical impedance spectroscopy

The effect of solution pH on the corrosion behavior of carbon steel and the structure of the passive film in the presence of 1 mmol L^{-1} concentration of both phosphate and chloride ($R = 1$) was studied using impedance method and the registered data in the form of Nyquist and Bode plots are shown in Fig. 2. At pH = 9 and 10, one time constant is identified from the impedance diagrams. This observation together with the active state of corrosion resulted from the polarization data (Fig. 1), support that the EIS data at pH = 9 and 10 correspond to the corrosion process at the metal/solution interface not to the formation of a stable passive film. The existence of two loops at the Nyquist plots for the higher pH values (11 and 12) indicates the development of a stable and strong passive film on the metal surface, as obtained by polariza-

tion method, where the loop at high frequencies is related to the characteristics of passive film and one at the low frequencies is attributed to the events occurred at the metal surface.

The fitting analysis was applied for the EIS spectra using the equivalent circuit models (ECMs) proposed in Fig. 3. The ECM, composed of a single electrical circle associated with the Warburg element (Fig. 3a), was used to simulate the corrosion behavior of carbon steel with an active state. The equivalent circuit with two electrical circles (Fig. 3b), which is similar to that applied by Yohai et al. [5,10], was used to analyze the impedance data in a passive state of corrosion. In the case of equivalent circuit with two electrical circles (Fig. 3b), the external circle is attributed to the formation of the passive film associated with an additional Warburg element characterized the diffusion phenomenon along the pores of the passive film, while the internal circle corresponds to the corrosion process occuring at the metal/passive film interface [10]. The impedance of Warburg element is expressed by the following equation [10,25]:

$$Z_w = \frac{W_R}{(\omega\, j\, T)^{0.5}} \tanh(\omega j T)^{0.5} \quad (1)$$

where ω is the angular frequency (rad/s), W_R is related to the diffusion resistance ($\Omega\ cm^2$), j defines the imaginary number $\left(\sqrt{-1}\right)$, and parameter T is relevant to the effective diffusion coefficient and the effective diffusion thickness (sec).

In these equivalent circuits (Fig. 3), R_s represents the solution resistance, R_f the ionic transfer resistance within the passive film pores and R_t describes the charge transfer resistance. The constant phase element (CPE) is frequently used instead of a pure capacitance element to deal with the non-homogeneity or porosity of the passive film and the metal/film interface denoted by CPE_f and CPE_t, respectively. The impedance of CPE is described by the following relation:

$$Z_{CPE} = \frac{1}{Y(\omega\, j)^n} \quad (2)$$

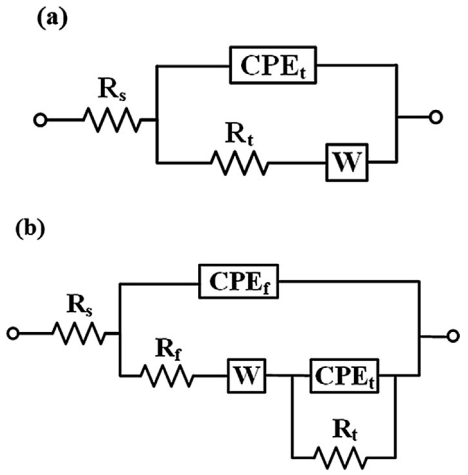

Fig. 3. Equivalent circuits used for analyzing the EIS data in: (a) the active state of corrosion and (b) the passive state of corrosion associated with diffusion process.

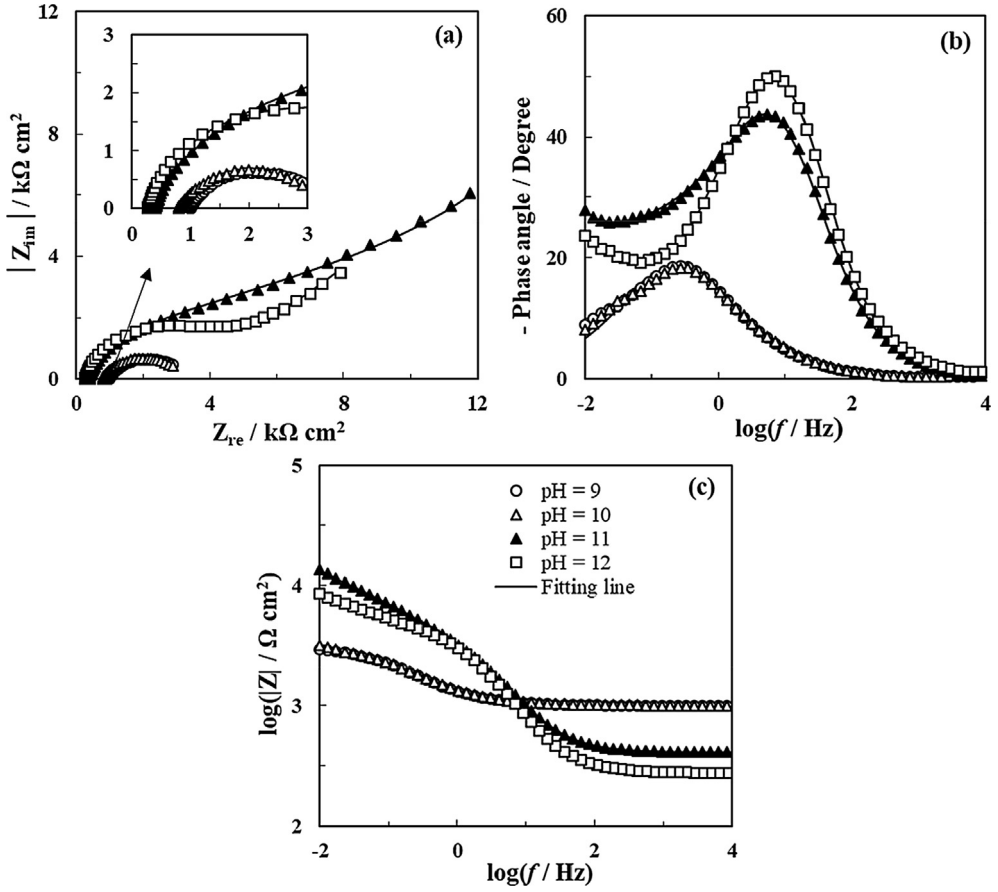

Fig. 2. Impedance spectra recorded on carbon steel surface in CPS1 at different pH values after 24 h immersion at 25 °C. The data presented in the form of (a) Nyquist plot, (b) and (c) Bode plots.

where Y is a pseudo-capacitance parameter ($s^n\ \Omega^{-1}\ cm^{-2}$) and n is the power constant of CPE. To evaluate the CPE behavior at high frequencies, the graphical method represents useful information about the CPE parameters and the appropriate equivalent circuit used to fitting analysis. In this study, for CPS1 and at pH = 9 through 12, the imaginary part of impedance ($|Z_{im}|$) as a function of applied frequency in logarithmic coordinates is plotted in Fig. 4. For all systems, a curvature is observed at the highest frequencies because of the current and potential distribution [36]. At pH = 9 and 10, the existence of one negative slope followed by an approximately flat region, suggesting the occurrence of one process and thus the ECM presented in Fig. 3a is valid. In this manner, at pH = 11 and 12, the presence of two negative slopes associated with a flat region at the intermediate frequencies, indicates the existence of two different processes and hence reflects the accuracy of the ECM shown in Fig. 3b.

Therefore, in this work, the CPE parameters including Y and n only for the CPE, corresponding to the high frequency region (from about 1 kHz to 0.3 Hz), were estimated using graphical method according to the procedure that was well addressed in the literature [36,43]. Note that after estimation of CPE parameters at the high frequency region, the value of other parameters was determined using the fitting procedure of impedance spectra with ECMs (Fig. 3) in Zview™ software.

In this study, the capacitance values of charge transfer layer (C_t) were calculated using the formula derived by Brug et al. [44] on the basis of surface distribution of time constants as following:

$$C_t = Y_t^{1/n_t}\left(\frac{R_s R_t}{R_s + R_t}\right)^{(1-n_t)/n_t} \quad (3)$$

While, the value of film capacitance (C_f) was obtained using the power-law model, developed by Hirschorn et al. [45,46] on the basis of the normal distribution of time constants as:

$$C_f = g\, Y_f (2\pi f_\delta)^{n_f - 1} \quad (4)$$

where f_δ is characteristic frequency (Hz), which is higher than the largest measured frequency (f_{max}). Therefore, f_{max} was applied to calculate maximum film capacitance [36,43,46]. Parameter g is described as the following equation [45,46]:

$$g = 1 + 2.88(1 - n_f)^{2.375} \quad (5)$$

With respect to these equations, the effect of solution pH on the impedance parameters for the corrosion of carbon steel in CPS1 was studied and the generated data are given in Table 3.

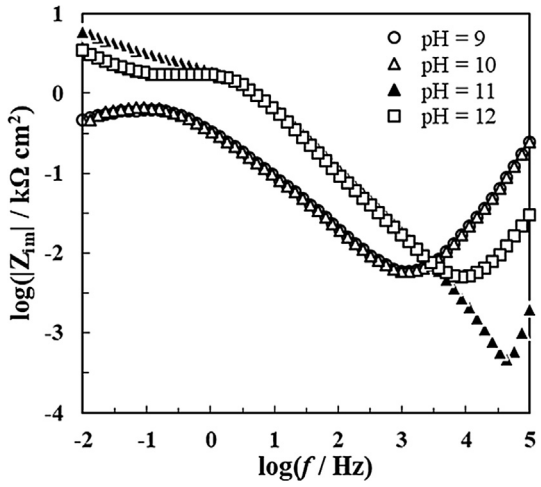

Fig. 4. Graphical representation of the imaginary part of impedance as a function of applied frequency in logarithmic coordinates for CPS1 at pH = 9 through 12.

According to Table 3, the increase of solution pH from 9 to 11 is associated with the increase of charge transfer resistance (R_t) and a significant decrease in C_t, indicating that the better protection against corrosive conditions and a completely passive state, is established at pH = 11, specified as the pH_p value in CPS1. However, for the pH greater than pH_p, R_t decreases and C_t increases, suggesting that the further increase in the concentration of hydroxyl groups has no improvement on the phosphate inhibition from the aspect of uniform corrosion. These trends of variations are in good agreement with those obtained by the polarization tests. Moreover, the effect of pH, varying from 11 to 12, on the parameters of R_t and C_t can be satisfied by the reduction of both R_f and W_R associated with the increase of C_f (Table 3). In this regard, the decrease of R_f can be explained by two main reasons: (a) the increment in the porosity of the surface film and (b) the change in the composition of the passive film. However, the increase of both n_f and C_f suggests the hypothesis that the decrement of R_f has been probably arisen from a decrease in the electronic property of passive film which is in consistent to the report of Yohai et al. [5,10]. This behavior can be interpreted by the competitive adsorption of different forms of phosphate along with hydroxyl groups at the metal/electrolyte surface which required to be further investigated later.

It should be noted that the value of C_t obtained for carbon steel in CPS1 at pH = 9 and 10, is too high from that would be expected for a double layer capacitance (less than 100 $\mu F\ cm^{-2}$) which can be interpreted by the polarizable state of pseudo-capacitance where the cation injection occurs through the interface film [24].

In the case of active state of corrosion, it is possible that the metal surface was partially covered by an oxide film. To have a feeling of the importance of this porous oxide film and hence the rightness of the fitting method, the capacitance value of an oxide film for such a system was estimated by assuming a CPE_f in parallel with CPE_t for the ECM proposed in Fig. 3a and the value of film capacitance (C_f) can be estimated by the following equation:

$$C_f = \frac{\varepsilon \varepsilon_0 A}{d} \quad (6)$$

where d is the film thickness assumed about 3 nm [47], ε_0 is the vacuum permittivity (8.854×10^{-14} F/cm), ε dielectric constant assumed to be about 12 [36,47,48], and A is the effective surface area where for an active state of corrosion it was considered as an arbitrary and enough low level (about 20 percent) of surface coverage, and the value of film capacitance was estimated by Eq. (6) to be equal 0.71 $\mu F\ cm^{-2}$. This value is almost two orders smaller than the capacitance value of the charge transfer layer which approves the rightness of fitting by the ECM (in Fig. 3a) used for the active state of corrosion.

The effect of phosphate and chloride concentration at an equimolar value ($R = 1$) and at the constant pH of 11, on the corrosion of carbon steel was studied using EIS experiment and the impedance curves in the form of Nyquist and Bode plots for CPS1, CPS10, and CPS100 are shown in Fig. 5. With respect to the shape of Nyquist diagrams together with the graphical analysis based on the plot of $|Z_{im}|$ as a function of applied frequency (not shown), it can be found that the circuit model with two-time constants (in Fig. 3b), is appropriate to fitting the EIS data for all solutions as well discussed before. The impedance parameters were estimated according to the procedure explained before on the basis of the graphical method and fitting analysis and the obtained data are given in Table 4.

It can be found that an equal increase in the concentration of both phosphate and chloride ions from 1 to 100 mmol L^{-1} causes a decrease in R_f and an increase in both film capacitance C_f and parameter n_f. These variations are like those obtained for the effect of the hydroxyl groups on the characteristic of the passive film

Table 3
Effect of solution pH on the impedance parameters estimated for the corrosion of carbon steel in CPS1 at 25 °C.

pH	R_s (Ω cm^2)	R_f (kΩ cm^2)	n_f	C_f (μF cm^{-2})	W_R (kΩ cm^2)	T (sec)	R_t (kΩ cm^2)	n_t	C_t (μF cm^{-2})
9	998	–	–	–	1.11	196	1.99	0.68	366
10	890	–	–	–	0.56	42	2.12	0.66	322
11	410	3.61	0.70	2.2	39.68	514	4.64	0.56	68
12	279	3.36	0.79	2.4	23.95	449	1.29	0.52	83

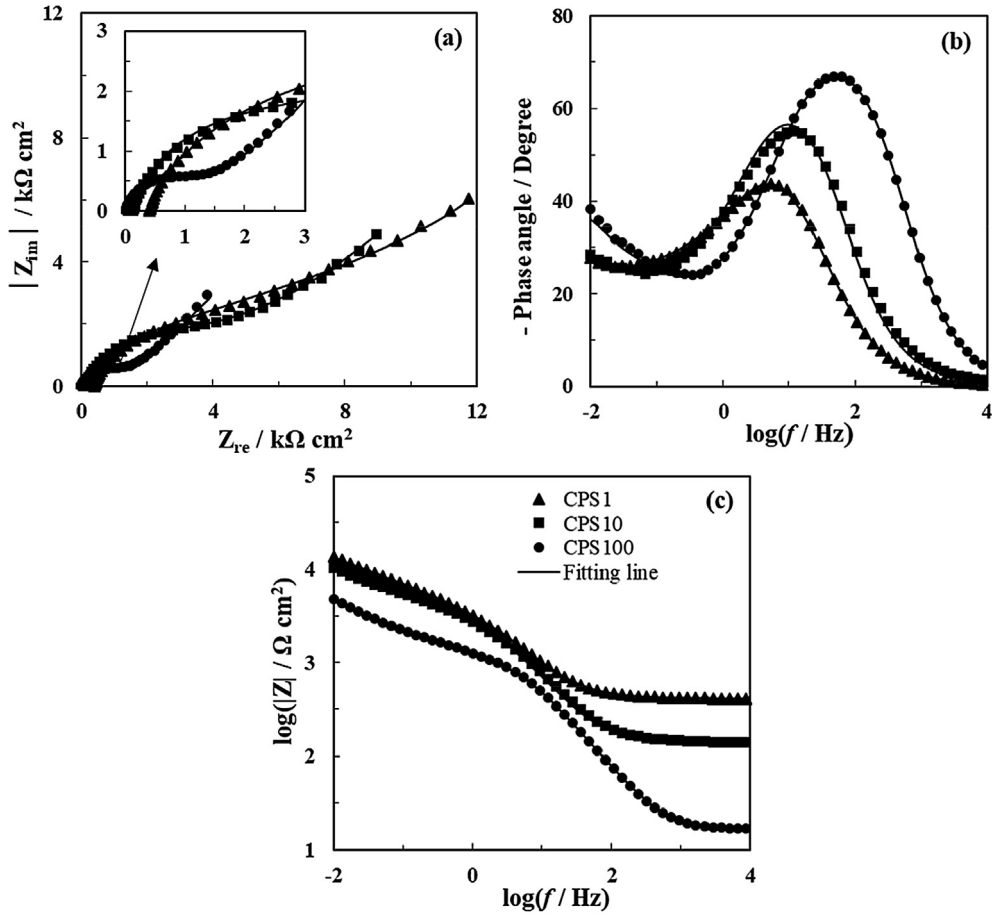

Fig. 5. Impedance spectra recorded on the carbon steel surface at pH = 11 in CPS1, CPS10, and CPS100 after 24 h immersion at room temperature. The data presented in the form of (a) Nyquist plot, (b) and (c) Bode plots.

(Table 3) and decrement of R_f can be related to the increment in the electrical nature of passive film probably due to the increase of the ion concentration within the pore solution of the passive film. Likewise, this explanation can be satisfied by the significant decrease of W_R from 39.68 to 9.49 kΩ cm^2 together with the decrease of solution resistance, R_s from 413 to 17 kΩ cm^2.

On the other hand, the increase of resistance against pitting corrosion as a result of an increase in E_{pit} (see Table 2), can be described by the higher level of compaction within the structure of passive film (increase of n_f), where reducing the penetration of aggressive ions towards the metal surface.

Furthermore, Table 3 shows that an increase in the amounts of both chloride and phosphate ions is associated with a decrease in R_t and increase in C_t values. These demonstrate the higher rate of uniform corrosion which is consistent with the polarization results (Table 2). In this regard, the highest value of W_R compared with the values of R_f, and R_t, advising that for a short time immersion, the diffusion phenomenon has a predominant effect on the corrosion process.

It was reported that the passivation of carbon steel in a simulated concrete pore solution and at a high pH value is a time-dependent process [49]. To check this, in the present work, the

Table 4
Impedance parameters estimated for corrosion of carbon steel in CPS1, CPS10, and CPS100 at pH = 11 and 25 °C.

Solution	R_s (Ω cm^2)	R_f (kΩ cm^2)	n_f	C_f (μF cm^{-2})	W_R (kΩ cm^2)	T (sec)	R_t (kΩ cm^2)	n_t	C_t (μF cm^{-2})
CPS1	413	3.61	0.70	2.2	39.68	514	4.64	0.56	68
CPS10	140	2.95	0.80	2.9	34.71	486	1.99	0.58	81
CPS100	17	1.01	0.87	7.5	9.49	105	0.29	0.65	94

EIS test was performed as an example in CPS1 at pH = 12 after 48 h, and the impedance curves recorded after 24 and 48 h for this system are shown in Fig. 6. It is obvious that there is no remarkable difference between the recorded data at least for the short term, indicating the immersion time of 24 h is suitable to form and grow the passive film; where is similar to that used by the other researchers [6,7,10].

3.3. Surface analysis by SEM/EDS

At the end of potentiodynamic polarization test, the corrosion state of carbon steel surface was evaluated by SEM and the surface components either in passive or in the active state were characterized by EDS analysis. The SEM images and EDS spectrum of the carbon steel surface in CPS1 at pH = 9, 11, and 12 are shown in Fig. 7. At pH = 9, the formation of big pits on the carbon steel surface is evident (Fig. 7a) probably due to the active state of corrosion, while at pH = 11 the pit size is markedly decreased by the passivation of metal surface but there is still a relatively high density of pits on the metal surface (Fig. 7b). However, further increase in pH up to 12 results a uniform surface without any sign of pit (Fig. 7c) due to the high resistance against pitting corrosion. Therefore, it can be stated that these observations are directly related to the corrosion state together with the change in the E_{pit} values obtained by the polarization test (Table 2).

Moreover, Fig. 7a and b show the presence of white zones inside the pit formed on the metal surface, and this can be related to the precipitation of phosphate species as a result of competition with chloride ions [24]. However, at pH = 12, a thin and relatively porous layer with white color is observed on the carbon steel surface at high magnification (Fig. 7c), recommended that an iron phosphate complex is also precipitated at the upper part of the passive film in the free pit zones as reported before [8–10].

The quantitative-elemental analysis of carbon steel surface using EDS spectra at different pH values reveals the presence of Fe, O and P elements at the regions without and with the pit (Fig. 7a through c) confirming that the passive film is composed of both iron (hydro)oxides and iron phosphate complexes. However, P concentration inside the pits is much higher than the regions without pit demonstrating the hypothesis that the chloride attack on the carbon steel surface triggers the phosphate ions to inhibit the pitting corrosion. Therefore, the white zones around the pit points observed by SEM images satisfy the existence of phosphate ions. Moreover, the P concentration on the metal surface, especially in the region without the pit, is less than that for O element, implying that the structure of passive film mainly consists of iron (hydro)oxides in alkaline solutions as described in detail elsewhere [22,28,50].

Fig. 8 shows the SEM images and EDS spectra for carbon steel in CPS10 and CPS100 at pH = 11. The effect of the amounts of chloride and phosphate at $R = 1$ and at the constant pH = 11 can be inspected by the comparison of Fig. 7b and 8. It is apparent from SEM images that both the size and density of pits are significantly decreased by an increase in the phosphate content from 1 to 100 mmol L^{-1}. This indicates that phosphate species could reduce both the initiation and growing stage of pitting corrosion, which is supported by the increase in the quantity of P element inside the pit according to the EDS analysis. These are in good agreement with the increase of pitting potential obtained by the polarization results (Table 2). The absence of chloride element in the EDS spectrum recorded at the pitting locations can be related to rinsing the samples after potentiodynamic tests and to the solubility of the iron/chloride salts within the electrolyte.

At the regions without pit, the elemental analysis of the passive film by EDS shows that the higher concentration of phosphate within solution bulk provides no significant difference in the weight percent of P element. Therefore, the contribution of phosphate species in the structure of passive film does not change with the phosphate concentration if it is used in an adequate quantity ($R = 1$) that required for efficient protection of uniform corrosion.

3.4. Weight loss measurement

The corrosion of carbon steel in the long term was inspected using the weight loss method in the aerated condition, according to ASTM D 2688 [39]. To this end, the carbon steel coupons were immersed in CPS1, CPS10, and CPS100 at pH_p for 120 days and the results of weight loss measurement are given in Table 5. The values of corrosion current density were calculated using Faraday's law as follows:

$$i_{corr} = \frac{(W_1 - W_2)F}{A, t\, EW} \tag{7}$$

where W_1 is the weight of coupon before immersion (gr) and W_2 is the weight of coupon after immersion (gr) following thoroughly removing the corrosion products from the surface of the coupons. Also, F is Faraday's constant (96500 C/eq), A is the coupon surface exposed to the corrosive media (cm^2), t is the aging time (sec), and EW is the equivalent weight (27.92 gr/eq for Fe).

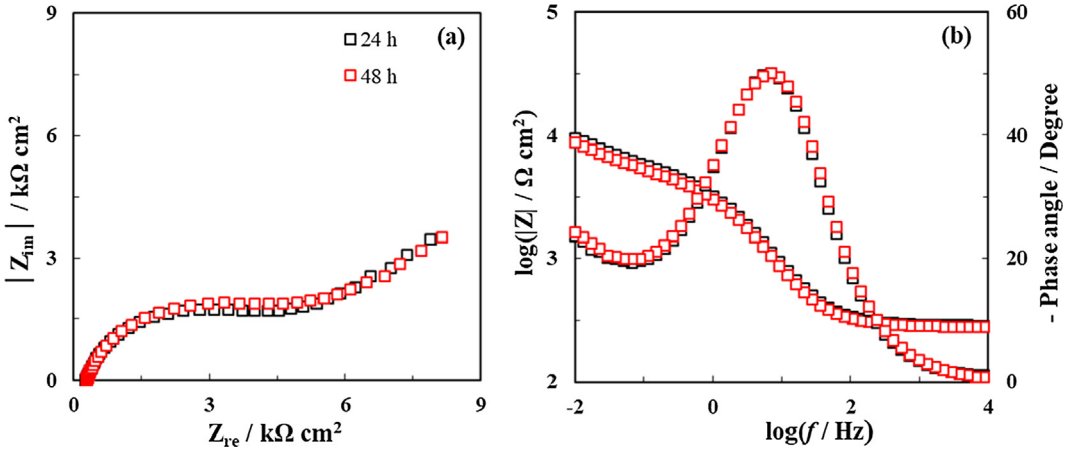

Fig. 6. Effect of exposure time on the Impedance spectra recorded on the carbon steel surface at pH = 12 for CPS1 after 24 and 48 h immersion at room temperature. The data presented in the form of (a) Nyquist plot and (b) Bode plots.

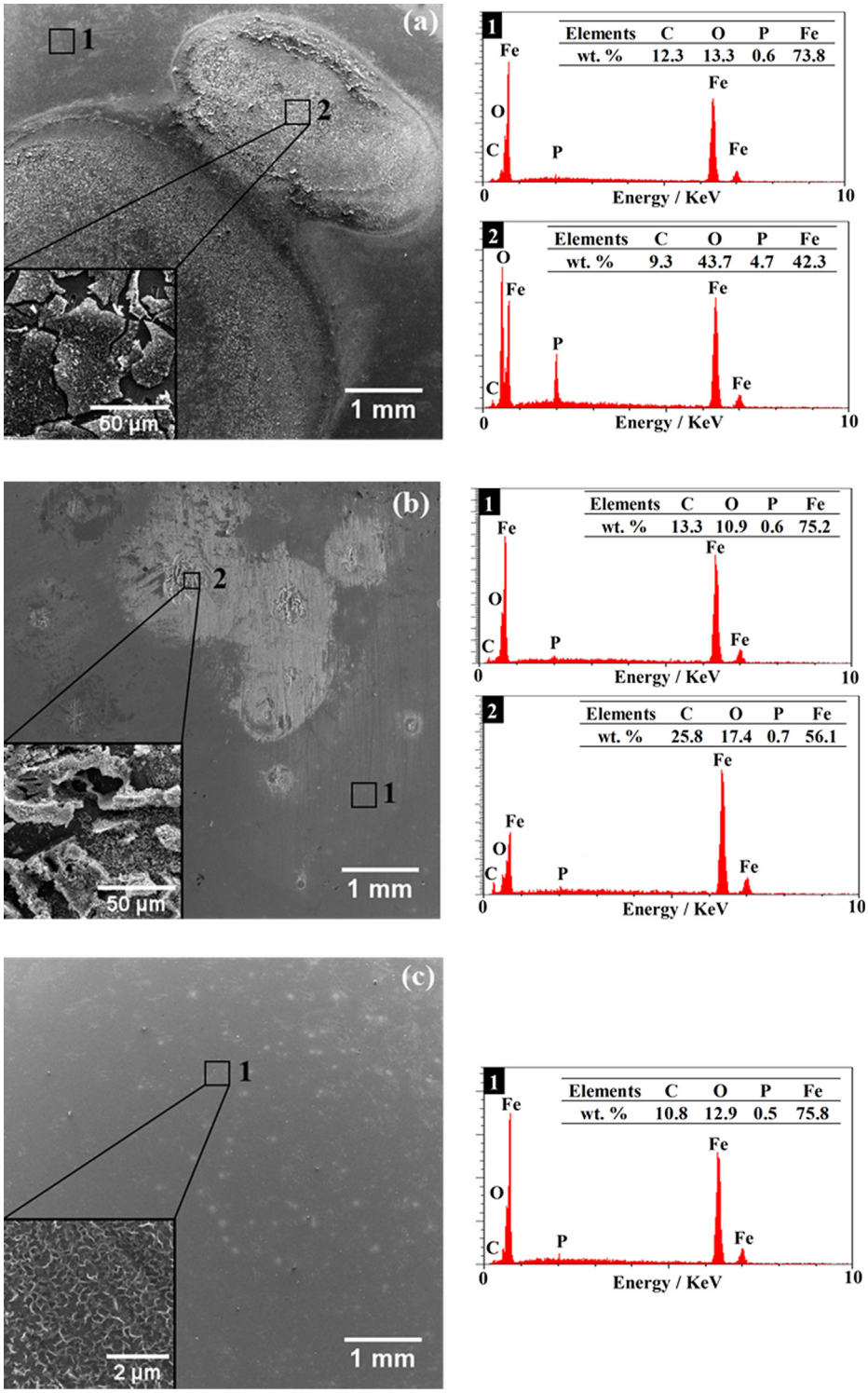

Fig. 7. SEM images and EDS spectra of the carbon steel surface after anodic polarization in CPS1 at: (a) pH = 9, (b) pH = 11, and (c) pH = 12 and at room temperature.

From the data given in Table 5, the corrosion current density, i_{corr}, is significantly decreased by a decrease in pH_p. This trend of variation agrees with that obtained by polarization measurement in a short time (Table 2). However, it is evident that the values of i_{corr}, estimated by weight loss in the long term (after 120 days) of exposure to electrolyte, are much lower than those obtained by polarization method in the short term (after 1 day), indicating the better performance of phosphate inhibitor in long term exposure.

Fig. 9 shows the photographs taken from coupons at the end of the immersion test. The color of corrosion products in CPS1 is dark brown (Fig. 9a), suggesting the formation of iron (hydro)oxides [51], while the light brown and yellowish color of corrosion products in CPS10 (Fig. 9b) can be attributed to the precipitation of iron phosphate complexes along with the iron (hydro)oxides [52]. These observations together with the weight loss measurements satisfies that the concentration of phosphate ions within the electrolyte plays an important role on the nature of passive film at the

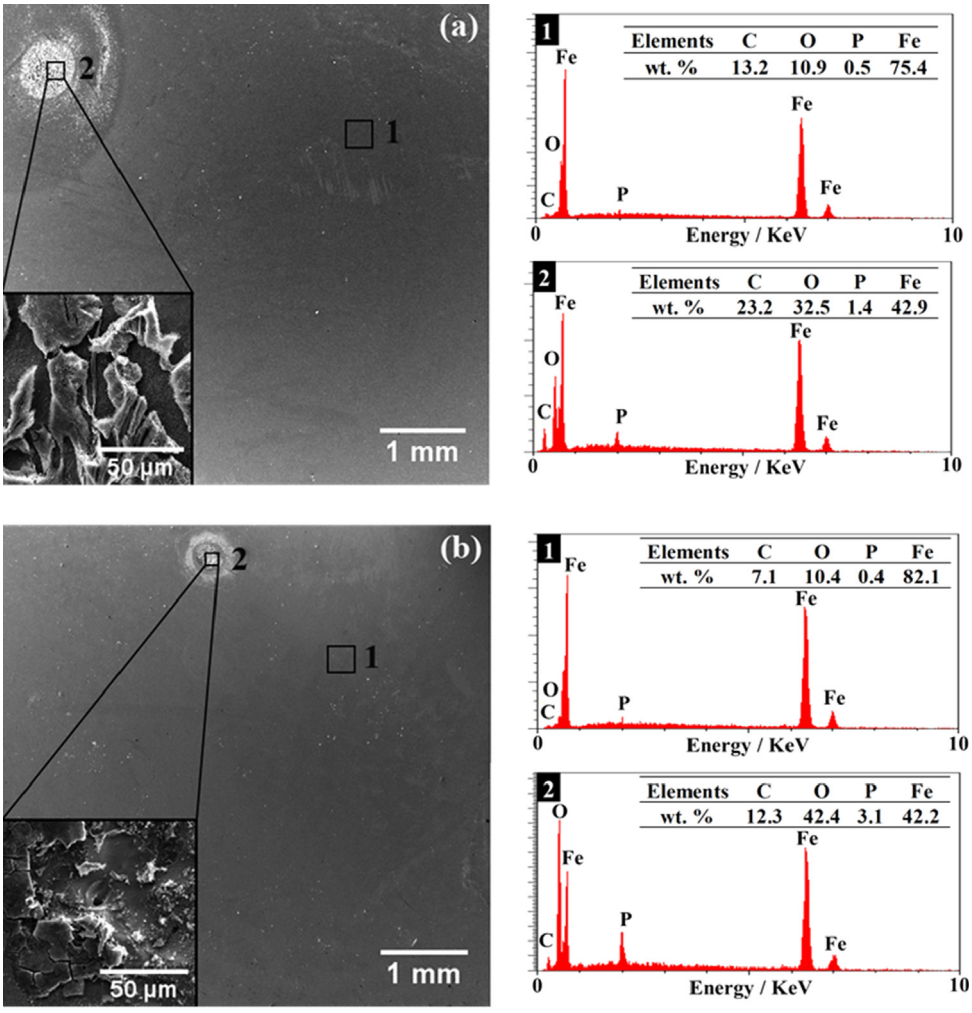

Fig. 8. SEM images and EDS spectra of the carbon steel surface after anodic polarization at pH = 11 in (a) CPS 10 and (b) CPS100, at room temperature.

Table 5
Weight loss data for carbon steel in CPS1, CPS10, and CPS100 at pH_p for 120 days immersion at room temperature.

Solution	pH_p	Weight loss (mgr)	i_{corr} (µA cm^{-2})
CPS1	11	203 ± 10	0.36 ± 0.02
CPS10	10	161 ± 14	0.29 ± 0.03
CPS100	9	19 ± 5	0.04 ± 0.01

pitting locations in long term exposure and hence the protection performance of phosphate ions is decreased by the low quantity of phosphate ions (CPS1). In this regard, in the case of coupon immersed in CPS100, presented in Fig. 9c, no corrosion product and pitting occurrence can be visually identified on the metal surface, demonstrating the excellent protection performance of phosphate ions in the long term at a high concentration as reported in the literature for concrete applications [10,25,30].

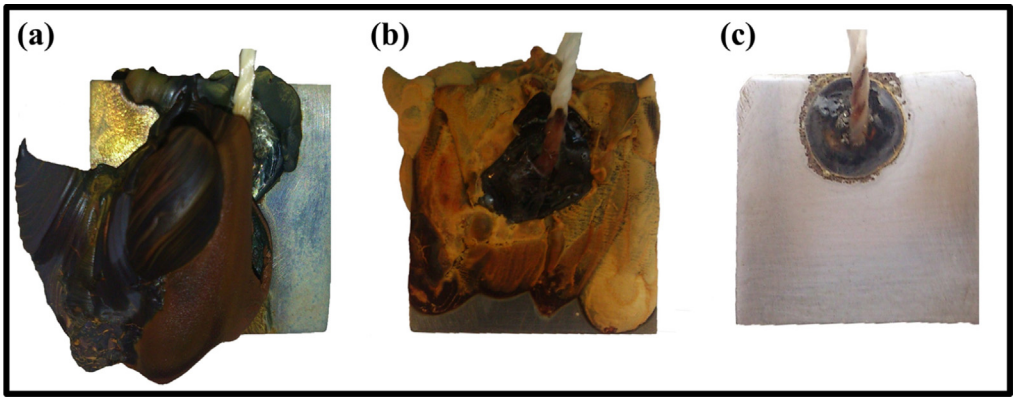

Fig. 9. Photographs of the specimens after 120 days immersion in (a) CPS1 at pH_p = 11, (b) CPS10 at pH_p = 10, and (c) CPS100 at pH_p = 9 and at room temperature.

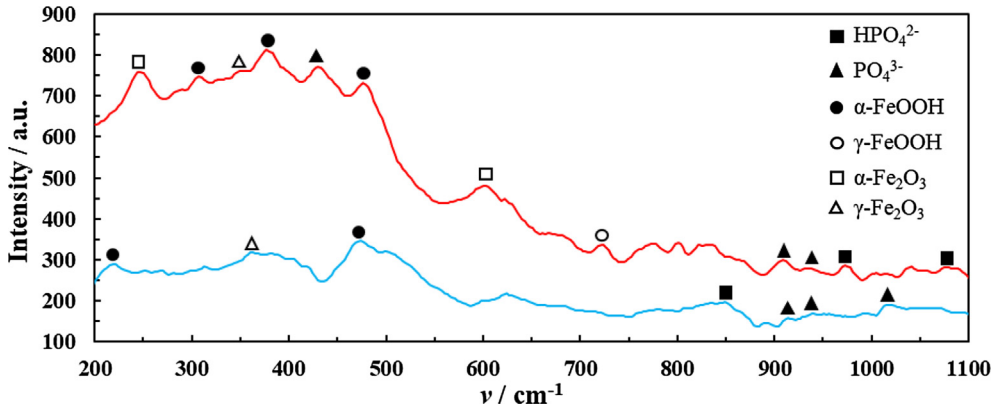

Fig. 10. Raman spectra of corrosion products formed on the carbon steel surface after 120 days immersion in CPS1 (red line) and CPS10 (blue line) at pH_p and at room temperature. (For interpretation of the references to color in this figure legend, the reader is referred to the web version of this article.)

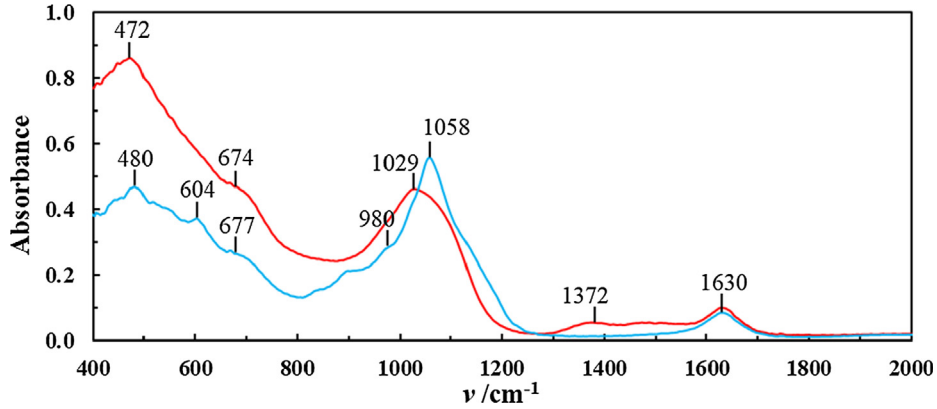

Fig. 11. FTIR spectrum of corrosion products after 120 days immersion in CPS1 (red line) and CPS10 (blue line) at pH_p and at room temperature. (For interpretation of the references to color in this figure legend, the reader is referred to the web version of this article.)

3.5. Raman spectroscopy and FTIR analysis

After weight loss measurement, Ex-situ Raman spectroscopy and FTIR were employed to identify the composition of corrosion products formed on the carbon steel coupons in CPS1 and CPS10.

Raman spectra (Fig. 10) show two bands centered at about 980 and 1080 cm^{-1} for CPS1 together with one at 850 cm^{-1} for CPS10, corresponding to the presence of hydrogen phosphate anions (HPO_4^{2-}) [24,53]. Phosphate anions (PO_4^{3-}) can be identified by the bands at 443, 910, 935, and 1020 cm^{-1} in both CPS1 and CPS10 [24,53]. Theses evidences are in good agreement with those reported by other researchers [10,24,53] and demonstrate the formation of iron phosphate complexes. Moreover, different iron (hydro)oxide compositions including goethite (α-FeOOH) at the bands about 220 cm^{-1}, 305 cm^{-1}, 382 cm^{-1}, and 475 cm^{-1} [54–56] and also maghemite (γ-Fe_2O_3) at band about 360 cm^{-1} can be detected in both CPS1 and CPS10 [56,57]. However, it appears that hematite (α-Fe_2O_3) at 250 and about 605 cm^{-1} [10,56] and lepidocrocite (γ-FeOOH) at 720 cm^{-1} [57] are formed in CPS1 which can be supposed as the higher contribution of iron (hydro) oxides in corrosion products as observed by the photographs (Fig. 9). The higher intensity of the Raman spectrum recorded for CPS1 than that for CPS10 has been likely arisen from the higher amounts of corrosion products as a result of greater corrosion rate [5,10].

Fourier transform infrared spectroscopy was conducted using an equal amount of corrosion products, formed in CPS1 and CPS10, and the recorded spectra are shown in Fig. 11. In both CPS1 and CPS10, the bands between 450 and 700 cm^{-1} characterize the presence of γ- Fe_2O_3 [58,59], while γ-FeOOH can be detected by a peak at about 1372 cm^{-1} [60] only in CPS1. These observations confirm the presence of iron(hydro)oxides in the corrosion products as obtained by Raman spectroscopy. Fig. 11 shows a broad band at 1029 cm^{-1} for CPS1 indicating the asymmetric stretching (F, υ_3) of phosphate anions, while in CPS10 there are two narrow bands at 980 and 1058 cm^{-1} [61,62] due to hydrogen phosphate anions with symmetric bonding (E, υ_2) and symmetric stretching (A_1, υ_1), respectively, as reported previously [62,63]. Besides, the same absorbance at 1630 cm^{-1} for both CPS1 and CPS10 can be attributed to the contribution of iron phosphate [60].

Since an equal quantity of corrosion products of CPS1 and CPS10 was utilized to FTIR analysis, a quantitative comparison can be made on the results. From this aspect, the peak intensities, corresponded to iron(hydro)oxides and iron phosphate complexes, are greater for CPS1 and CPS10, respectively; which can be taken into account as the higher contribution of these compounds in the corrosion products and is consistent with the color of corrosion products shown in Fig. 9.

4. Conclusions

The effect of solution pH on the performance of phosphate inhibitor in different concentrations of phosphate but at one-to-one phosphate to chloride molar ratio ($R = 1$) was well investigated using the electrochemical and surface analysis methods, and the main results as follows:

- When the concentration of hydroxyl groups increases, at a certain pH named as passivation pH (pH_p), the corrosion state changes from active to passive. However, the value of pH_p depends on the amounts of phosphate and chloride concentrations.
- Generally, the electrochemical data showed that the increase of both phosphate and chloride ions facilitates the passivation in the lower pH_p, reflecting the synergistic effect between phosphate ions and hydroxyl groups to form a passive film on the surface of carbon steel. However, when the passive film established on the metal surface, an increase in both hydroxyl and phosphate concentrations has no improvement on the uniform corrosion in the short term, while both the polarization results and SEM images indicated an increase in the resistance of passive film against pitting corrosion.
- In the long term, both weight loss and corrosion products analysis confirmed that the addition of higher amounts of phosphate, i.e., 100 mmol L^{-1} at $R = 1$, favors the protection of metal surface against both uniform and pitting corrosion. In other words, at the low chloride contamination, the R ratio of 1 is not adequate to create a reliable protection of carbon steel against corrosion phenomenon.
- The surface analysis methods demonstrated that the inhibition mechanism of phosphate ions is attributed to the formation of a passive film with a duplex layer on the metal surface, including the inner layer of iron(hydro)oxides, formed by a solid-state mechanism, and the outer layer of iron phosphate complexes mainly as $FeHPO_4$, $Fe_3(PO_4)_2$ and even $Fe(PO_4)$, formed via a dissolution-precipitation mechanism.
- The concentration of phosphate species inside the pits was higher than the passive film zones without the pit. This indicates that phosphate ions could inhibit the corrosion process through a competitive adsorption mechanism with chloride ions where the more chloride attack triggers the phosphate species to further adsorb at the pit locations on the metal surface.

Declaration of Competing Interest

The authors declare that they have no known competing financial interests or personal relationships that could have appeared to influence the work reported in this paper.

Acknowledgment

We want to thank Khorasan Razavi Gas Co. for providing us with laboratory facilities required for conducting the experiments for the present study.

References

[1] S.M. Abd El Haleem, S. Abd El Wanees, E.E. Abd El Aal, A. Diab, Environmental factors affecting the corrosion behavior of reinforcing steel II. Role of some anions in the initiation and inhibition of pitting corrosion of steel in $Ca(OH)_2$ solutions, Corros. Sci. 52 (2010) 292–302.
[2] T. Söylev, M. Richardson, Corrosion inhibitors for steel in concrete: State-of-the-art report, Constr. Build. Mater. 22 (2008) 609–622.
[3] A. Douche-Portanguen, W. Prince, T. Lutz, G. Arliguie, Detection or quantitative analysis of a corrosion inhibitor, the sodium monofluorophosphate, in concrete, Cem. Concr. Compos. 27 (2005) 679–687.
[4] J. Shi, W. Sun, Effects of phosphate on the chloride-induced corrosion behavior of reinforcing steel in mortars, Cem. Concr. Compos. 45 (2014) 166–175.
[5] L. Yohai, M. Vázquez, M. Valcarce, Phosphate ions as corrosion inhibitors for reinforcement steel in chloride-rich environments, Electrochim. Acta 102 (2013) 88–96.
[6] M. Reffass, R. Sabot, M. Jeannin, C. Berziou, P. Refait, Effects of phosphate species on localised corrosion of steel in $NaHCO_3$ + NaCl electrolytes, Electrochim. Acta 54 (2009) 4389–4396.
[7] N. Etteyeb, L. Dhouibi, H. Takenouti, M. Alonso, E. Triki, Corrosion inhibition of carbon steel in alkaline chloride media by Na_3PO_4, Electrochim. Acta 52 (2007) 7506–7512.
[8] H.B. Mansour, L. Dhouibi, H. Idrissi, Effect of Phosphate-based inhibitor on prestressing tendons corrosion in simulated concrete pore solution contaminated by chloride ions, Constr. Build. Mater. 171 (2018) 250–260.
[9] H. Nahali, H.B. Mansour, L. Dhouibi, H. Idrissi, Effect of Na_3PO_4 inhibitor on chloride diffusion in mortar, Constr. Build. Mater. 141 (2017) 589–597.
[10] L. Yohai, W. Schreiner, M. Valcarce, M. Vázquez, Inhibiting steel corrosion in simulated concrete with low phosphate to chloride ratios, J. Electrochem. Soc. 163 (2016) C729–C737.
[11] H. Nahali, L. Dhouibi, H. Idrissi, Effect of Na_3PO_4 addition in mortar on steel reinforcement corrosion behavior in 3% NaCl solution, Constr. Build. Mater. 78 (2015) 92–101.
[12] D.M. Bastidas, M. Criado, S. Fajardo, A. La Iglesia, J.M. Bastidas, Corrosion inhibition mechanism of phosphates for early-age reinforced mortar in the presence of chlorides, Cem. Concr. Compos. 61 (2015) 1–6.
[13] D.M. Bastidas, M. Criado, V. La Iglesia, S. Fajardo, A. La Iglesia, J. Bastidas, Comparative study of three sodium phosphates as corrosion inhibitors for steel reinforcements, Cem. Concr. Compos. 43 (2013) 31–38.
[14] J.J. Shi, W. Sun, Electrochemical and analytical characterization of three corrosion inhibitors of steel in simulated concrete pore solutions, Int. J. Min. Metal. Mat. 19 (2012) 38–47.
[15] N. Etteyeb, M. Sanchez, L. Dhouibi, C. Alonso, C. Andrade, E. Triki, Corrosion protection of steel reinforcement by a pretreatment in phosphate solutions: assessment of passivity by electrochemical techniques, Corros. Eng., Sci. Technol. 41 (2006) 336–341.
[16] C. Volk, E. Dundore, J. Schiermann, M. Lechevallier, Practical evaluation of iron corrosion control in a drinking water distribution system, Water Res. 34 (2000) 1967–1974.
[17] H. Kumar, V. Saini, D. Kumar, R. Chaudhary, Influence of trisodium phosphate (TSP) antiscalant on the corrosion of carbon steel in cooling water systems, Indian, J. Chem. Technol. 16 (2009) 401–410.
[18] Y.S. Kim, W.C. Kim, J.G. Kim, Bulging rupture and caustic corrosion of a boiler tube in a thermal power plant, Eng. Fail. Anal. 104 (2019) 560–567.
[19] F. Daneshvar Fatah, A. Mostafaei, R. Hosseinzadeh-Taghani, F. Nasirpouri, Caustic corrosion in a boiler waterside tube: root cause and mechanism, Eng. Fail. Anal. 28 (2013) 69–77.
[20] B. Hakansson, P.-E. Augustsson, N.-G. Vannerberg, The influence of phosphate ions on the polarisation behaviour of iron, Electrochim. Acta 28 (1983) 791–799.
[21] V.S. Muralidharan, K.S. Rajagopalan, Kinetics and mechanism of passivation of steel in sodium phosphate solutions, Electrochim. Acta 23 (1978) 1297–1302.
[22] J. Lumsden, Z. Szklarska-Smialowska, The properties of films formed on iron exposed to inhibitive solutions, Corrosion 34 (1978) 169–176.
[23] J. Mayne, J. Menter, The mechanism of inhibition of the corrosion of iron by solutions of sodium phosphate, borate, and carbonate, J. Chem. Soc. 103–107 (1954).
[24] A. Mohagheghi, R. Arefinia, Corrosion inhibition of carbon steel by dipotassium hydrogen phosphate in alkaline solutions with low chloride contamination, J Constr. Build. Mater. 187 (2018) 760–772.
[25] L. Yohai, W. Schreiner, M. Vázquez, M.B. Valcarce, Phosphate ions as effective inhibitors for carbon steel in carbonated solutions contaminated with chloride ions, Electrochim. Acta 202 (2016) 231–242.
[26] L. Sail, F. Ghomari, A. Khelidj, A. Bezzar, O. Benali, The effect of phosphate corrosion inhibitor on steel in synthetic concrete solutions, Adv. Mater. Res. 2 (2013) 155–172.
[27] V. Sastri, R. Packwood, Surface analysis in corrosion inhibition mechanisms, Mater. Corros. 38 (1987) 77–82.
[28] Z. Szklarska-Smialowska, R. Staehle, Ellipsometric study of the formation of films on iron in orthophosphate solutions, J. Electrochem. Soc. 121 (1974) 1393–1401.
[29] L. Dhouibi, E. Triki, M. Salta, P. Rodrigues, A. Raharinaivo, Studies on corrosion inhibition of steel reinforcement by phosphate and nitrite, Mater. Struct. 36 (2003) 530–540.
[30] L. Dhouibi, E. Triki, A. Raharinaivo, G. Trabanelli, F. Zucchi, Electrochemical methods for evaluating inhibitors of steel corrosion in concrete, Br. Corros. J. 35 (2000) 145–149.
[31] S. Refaey, S.A. El-Rehim, F. Taha, M. Saleh, R. Ahmed, Inhibition of chloride localized corrosion of mild steel by PO_4^{3-}, CrO_4^{2-}, MoO_4^{2-}, and NO_2^- anions, App. Surf. Sci. 158 (2000) 190–196.
[32] C. Shun'an, Z. Qing, Z. Zhixin, A study of the influence of chloride ion concentration on the corrosion behavior of carbon steel in phosphate high-temperature boiler water chemistries, Anti-Corros. Methods and Materials 55 (2008) 15–19.
[33] L.B. Niu, K.J.C.S. Nakada, Effect of chloride and sulfate ions in simulated boiler water on pitting corrosion behavior of 13Cr steel, 96 (2015) 171-177.
[34] H. Khani, R. Arefinia, Inhibition mechanism of nitrite on the corrosion of carbon steel in simulated cooling water systems, Mater. Corros. 69 (2018) 337–347.
[35] H. Nahali, L. Dhouibi, H. Idrissi, Effect of phosphate based inhibitor on the threshold chloride to initiate steel corrosion in saturated hydroxide solution, Constr. Build. Mater. 50 (2014) 87–94.
[36] L. Hamadou, L. Aïnouche, A. Kadri, S.A.A. Yahia, N. Benbrahim, Electrochemical impedance spectroscopy study of thermally grown oxides exhibiting constant phase element behaviour, Electrochim. Acta 113 (2013) 99–108.

[37] ASTM G5-94, Standard Reference Test Method for Making Potentiostatic and Potentiodynamic Anodic Polarization Measurements, ASTM international (1999).
[38] ASTM G106-89, Standard Practice for Verification of Algorithm and Equipment for Electrochemical Impedance Measurements, ASTM international (1999).
[39] ASTM D2688, Standard Test Methods for Corrosivity of Water in the Absence of Heat Transfer (Weight Loss Methods), ASTM international (1999).
[40] S.A.M. Refaey, Inhibition of steel pitting corrosion in HCl by some inorganic anions, App. Surf. Sci. 240 (2005) 396–404.
[41] E. McCafferty, Introduction to corrosion science, Springer, 2010.
[42] K.K. Sharma, R.N. Deo, A. Kumar, K. Mamun, Rebar corrosion due to chlorides in synergy with sodium, potassium, and magnesium, Constr. Build. Mater. 165 (2018) 533–540.
[43] J. Baux, N. Caussé, J.R.M. Esvan, S. Delaunay, J. Tireau, M. Roy, D. You, N. Pébère, Impedance analysis of film-forming amines for the corrosion protection of a carbon steel, Electrochim. Acta 283 (2018) 699–707.
[44] G. Brug, A. Van Den Eeden, M. Sluyters-Rehbach, J. Sluyters, The analysis of electrode impedances complicated by the presence of a constant phase element, J. Electroanal. Chem. Interfacial Electrochem. 176 (1984) 275–295.
[45] B. Hirschorn, M.E. Orazem, B. Tribollet, V. Vivier, I. Frateur, M. Musiani, Constant-phase-element behavior caused by resistivity distributions in films I. Theory, J. Electrochem. Soc. 157 (2010) C452–C457.
[46] B. Hirschorn, M.E. Orazem, B. Tribollet, V. Vivier, I. Frateur, M. Musiani, Constant-phase-element behavior caused by resistivity distributions in films II. Applications, J. Electrochem. Soc. 157 (2010) C458–C463.
[47] A. Carnot, I. Frateur, S. Zanna, B. Tribollet, I. Dubois-Brugger, P. Marcus, Corrosion mechanisms of steel concrete moulds in contact with a demoulding agent studied by EIS and XPS, Corros. Sci. 45 (2003) 2513–2524.
[48] L. Hamadou, A. Kadri, N. Benbrahim, Characterisation of passive films formed on low carbon steel in borate buffer solution (pH 9.2) by electrochemical impedance spectroscopy, App. Surf. Sci. 252 (2005) 1510–1519.
[49] H. Torbati-Sarraf, A. Poursaee, Study of the passivation of carbon steel in simulated concrete pore solution using scanning electrochemical microscope (SECM), Materialia 2 (2018) 19–22.
[50] I.V. Sieber, H. Hildebrand, S. Virtanen, P. Schmuki, Investigations on the passivity of iron in borate and phosphate buffers, pH 8.4, Corros. Sci. 48 (2006) 3472–3488.
[51] A. Scheinost, U. Schwertmann, Color identification of iron oxides and hydroxysulfatesuse and limitations, 5 (1999) 1463-1471.
[52] H. Galal-Gorchev, W. Stumm, N. Chemistry, The reaction of ferric iron with ortho-phosphate, J. Inorg. Nucl. Chem. 25 (1963) 567–574.
[53] S. Simard, M. Odziemkowski, D. Irish, L. Brossard, H. Ménard, In situ micro-Raman spectroscopy to investigate pitting corrosion product of 1024 mild steel in phosphate and bicarbonate solutions containing chloride and sulfate ions, J. Appl. Electrochem. 31 (2001) 913–920.
[54] M. Valcarce, C. López, M. Vázquez, The role of chloride, nitrite and carbonate ions on carbon steel passivity studied in simulating concrete pore solutions, J. Electrochem. Soc. 159 (2012) C244–C251.
[55] B. Díaz, S. Joiret, M. Keddam, X. Nóvoa, M. Pérez, H. Takenouti, Passivity of iron in red mud's water solutions, Electrochim. Acta 49 (2004) 3039–3048.
[56] A. Hugot-Le Goff, J. Flis, N. Boucherit, S. Joiret, J. Wilinski, Use of Raman spectroscopy and rotating split ring disk electrode for identification of surface layers on iron in 1M NaOH, J. Electrochem. Soc. 137 (1990) 2684–2690.
[57] D. De Faria, S. Venâncio Silva, M. De Oliveira, Raman microspectroscopy of some iron oxides and oxyhydroxides, J. Raman Spectrosc. 28 (1997) 873–878.
[58] G. Gunasekaran, L. Chauhan, Eco friendly inhibitor for corrosion inhibition of mild steel in phosphoric acid medium, Electrochim. Acta 49 (2004) 4387–4395.
[59] N. Nakayama, A. Obuchi, Inhibitory effects of 5-aminouracil on cathodic reactions of steels in saturated $Ca(OH)_2$ solutions, Corros. Sci. 45 (2003) 2075–2092.
[60] S. Nasrazadani, The application of infrared spectroscopy to a study of phosphoric and tannic acids interactions with magnetite (Fe_3O_4), goethite (α-FeOOH) and lepidocrocite (γ-FeOOH), Corros. Sci. 39 (1997) 1845–1859.
[61] Y. Arai, D.L. Sparks, ATR–FTIR spectroscopic investigation on phosphate adsorption mechanisms at the ferrihydrite–water interface, J. Colloid Interface Sci. 241 (2001) 317–326.
[62] P. Persson, N. Nilsson, S. Sjöberg, Structure and bonding of orthophosphate ions at the iron oxide–aqueous interface, J. Colloid Interface Sci. 177 (1995) 263–275.
[63] J.M. Arroyave, V. Puccia, G.P. Zanini, M.J. Avena, Surface speciation of phosphate on goethite as seen by InfraRed Surface Titrations (IRST), Spectrochim. Acta, Part A 199 (2018) 57–64.